American Journal of Polymer Science and Technology
2026, Vol. 12, No. 2, pp. 51–70
https://doi.org/10.11648/j.ajpst.20261202.12

Research Article

# Simultaneous Optimization of Manufacturing Variables for 3D-Printed PETG Prototypes Leveraging Taguchi-Coupled Grey Relational Approach

**Abera Ayza Anebo[1, *], Temesgen Hailegiorgis Abebe[2], Devendra Kumar Sinha[3]**

[1]Department of Mechanical Engineering (Manufacturing Engineering Specialization), Wolaita Sodo University, Wolaita Sodo, Ethiopia

[2]Department of Mechanical Engineering (Industrial Engineering Specialization), Wolaita Sodo University, Wolaita Sodo, Ethiopia

[3]Department of Mechanical Engineering, Adama Science and Technology University, Adama, Ethiopia

## Abstract

This study investigates the optimization of Fused Deposition Modeling (FDM) parameters for Polyethylene Terephthalate Glycol (PETG) a material widely utilized in clinical and biomedical applications due to its favorable combination of lightweight properties, durability, and versatility. By applying a Grey-Taguchi methodology, the research systematically addresses how manufacturing variables influence mechanical performance, specifically focusing on tensile and compressive strength. Through rigorous signal-to-noise (S/N) ratio evaluations, the investigation identified the optimal parameter settings for individual mechanical properties. For tensile strength, a peak performance of 48.264MPa was achieved using level 1 extrusion temperature, a 55% infill density, and a printing speed of 20mm/s. Conversely, maximizing compressive strength to 47.762MPa required level 1 extrusion temperature, a higher infill density of 60%, and an increased printing speed of 30mm/s. Analysis of Variance (ANOVA) further confirmed that extrusion temperature, infill density, and printing speed all exert a statistically significant influence on these mechanical outcomes. Because biomedical and clinical components often require a balance of multiple mechanical traits, the study utilized Grey Relational Analysis (GRA) to establish a multi-response setting configuration of 1-3-3. This configuration yielded a peak grey relational grade of 1, representing the ideal compromise and overall optimal condition for dual-performance requirements. To ensure reliability, experimental validation tests were conducted. The results showed error margins of 4.01% for tensile strength and 6.14% for compressive strength. Because both error values remain well within acceptable engineering thresholds, the findings successfully verify the efficacy and precision of this optimization framework for additive manufacturing applications.

## Keywords

Additive Manufacturing, ASTM, 3D Printing, FDM, PETG, Tensile Strength

*Correspondence: Abera Ayza Anebo (aberaayza4@gmail.com)

**Received:** 8 August 2026; **Accepted:** 24 August 2026; **Published:** 22 September 2026

# 1. Introduction

Additive manufacturing (AM) constructs three-dimensional objects progressively by depositing material in successive layers, contrasting with conventional subtractive techniques like turning or milling that carve parts out of bulk stock. Originating in the 1980s when Chuck Hull pioneered stereolithography (SLA) at 3D Systems using a UV laser to cure photopolymer resins the field has since diversified into various commercialized methods, including selective laser melting (SLM) for metallic powders and fused deposition modeling (FDM/FFF) for extruded thermoplastics. FDM represents a widely adopted material extrusion approach where feedstock filaments pass through a heated nozzle, melting and depositing successively while the print bed adjusts vertically layer by layer. Popularized in affordable desktop and hobbyist machines, AM expanded rapidly into industrial sectors like automotive and aerospace during the 2000s, drastically cutting prototyping timelines and expenses through the introduction of high-grade engineering polymers and metal alloys.

In recent years, the swift progression of 3D printing techniques has unlocked transformative applications across biomedical, aerospace, construction, energy, and general industrial domains, with each sector customizing printing protocols and material inputs to meet unique operational demands. Capable of handling polymers, metals, ceramics, composites, and biological tissues, AM eliminates the need for expensive conventional tooling while enabling the fabrication of highly complex, lightweight geometries [3].

While early applications focused primarily on rapid prototyping and design iterations, enhancements in material quality and performance have shifted its role toward end-use manufacturing, highlighted by critical aerospace parts and customized patient-specific medical implants [7].

Extrusion-based AM, or FDM, continues to command significant research attention, operating by feeding thermoplastic filaments into a heated liquefier block before dispensing them through a precise nozzle to cool and solidify into continuous tracks governed by coordinated X, Y, and Z-axis motion derived from digital CAD files [4].

The primary benefits of additive manufacturing encompass:

1) Simplicity in operation and learning curve
2) Lowered manufacturing expenses and cycle times
3) Decreased raw material waste
4) Fabrication of lightweight parts
5) Minimized assembly requirements
6) Direct translation of digital designs
7) Fast progression from initial prototype to final production
8) Reduced environmental and energy footprints

# 2. Literature Review

This chapter reviews foundational studies concerning lattice structures, energy absorption, tensile evaluations, and compression behavior, focusing specifically on work examining thirty selective laser melting (SLM)-fabricated Ti-6Al-4V cellular components.

This research evaluated how fabrication techniques influence structural morphology and void percentages, revealing that actual porosity levels fell short of theoretical targets due to dimensional variances namely, oversized struts (especially along lateral boundaries) coupled with voids matching original design parameters. Mechanical evaluations demonstrated that stiffness and strength diminished predictably as porosity increased, though samples sharing identical porosity levels still displayed diverse mechanical responses dictated by pore geometry, distribution, and strut dimensions. Comparative analyses between tension and compression modes indicated that while tensile strength was lower, tensile stiffness increased markedly, and wear evaluations confirmed strong resistance across all configurations despite the need for deeper analysis regarding friction performance. Additionally, prior literature explored the energy-dissipating properties of aluminum foam sandwich (AFS) panels increasingly favored in automotive crash protection for their lightweight design and impact mitigation. Through a series of compression trials varying core thicknesses, stress-strain plotting showed that energy absorption scaled substantially from 12.74 J to 64.42 J, confirming the viability of AFS components for advanced vehicle safety structures [10].

# 3. Materials and Methodology

This investigation explored how varying nozzle temperatures influence the mechanical characteristics of PETG 3D-printed components. Using a Prusa i3 MK3S+ machine, the study fabricated standard dog-bone and compression test specimens across three distinct extrusion temperatures, producing a total of nine samples with three identical replicates per temperature setting. Through standardized mechanical testing, the research sought to clarify how thermal variations during extrusion impact the overall strength and structural behaviour of printed parts.

## 3.1. Equipment's

***Table 1.*** *List of equipment and machines utilized in the study.*

| S. No | Device Name | Purpose of usage |
|---|---|---|
| 1 | Prusa i3 MK3S+3D printer | To Produce the 3D printed PETG specimen |
| 2 | Hydraulic universal servo testing machine | To test the compression and tensile strength |

The selected material mentioned in above Table 1 used in the experiment was nine specimen of Polyethylene terephthalate glycol (PETG) filament, in the diameter of 1.75mm and fabricated PETG specimens in dimension of 115x20x7mm. One of the most common materials that are be use by industry as well as academic institutes is PETG. PETG (Polyethylene terephthalate glycol) are a common thermoplastic and is made from renewable sources such as corn starch and polymers.

## 3.2. Method

### 3.2.1. Fabrication Using the Prusa i3 MK3S+ 3D Printer

The design procedure commenced by establishing fundamental operational parameters to construct the required physical geometry. Once modeling was completed, the digital blueprints were converted into G-code to direct the precise movement paths of the print nozzle. Initial CAD software exports the digital model as an STL file, breaking down the outer surface geometry into a mesh of triangles. This STL file then serves as the primary input for the slicing program specifically open-source Ultimaker CURA to generate the required machine code.

Although alternative applications, such as depositing polymers directly onto textile bases to impart specialized traits like targeted stiffness, decorative features, or device mounting, are gaining research attention, their foundational workflow mirrors standard FDM processes with minor adjustments. For this study, all test specimens were digitally modelled using SolidWorks. The resulting CAD files were exported in stereolithography (STL) format and loaded into slicing software (such as Flash Print) to configure printing settings and divide the model into individual strata. The slicer then converts the STL input into a G-code file, enabling the printer to execute layer-by-layer material deposition, yielding the final tension and compression test specimens according to the American Society for Testing and Materials (ASTM) D638-I standard.

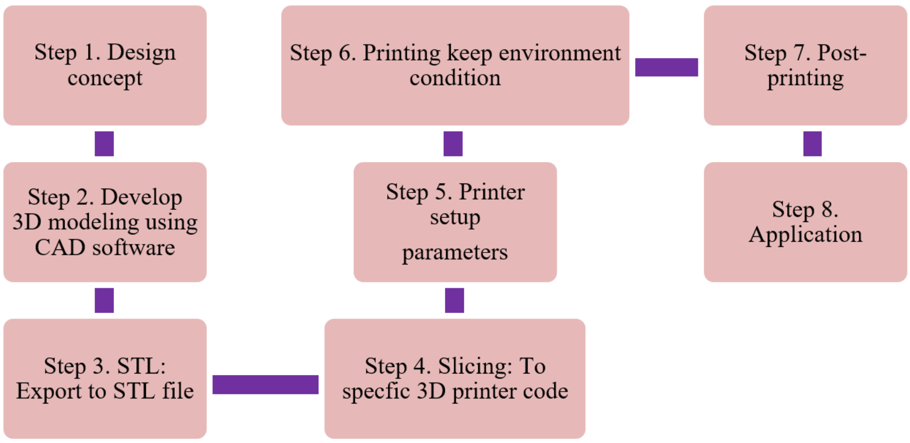


***Figure 1.*** *Work flow of Prusa i3 MK3S+3D printer machine.*

*Step 1 - CAD*

A CAD (computer-aided design) model is a digital A computer-aided design (CAD) model represents the external geometry of an object created using specialized software, such as SolidWorks (as illustrated in Figure 2). A CAD model consists of a series of interconnected geometric shapes, including polygons and curved surfaces. When creating a model from scratch in a dedicated program, the native file format is typically proprietary to maintain market differentiation and software compatibility.

However, standard CAD software allows users to export models into universal formats such as STL, .OBJ, or STEP. While these universal formats preserve the geometry for downstream applications, they do not retain the underlying construction history such as the specific parametric operations, features, and sketches used to build the model.

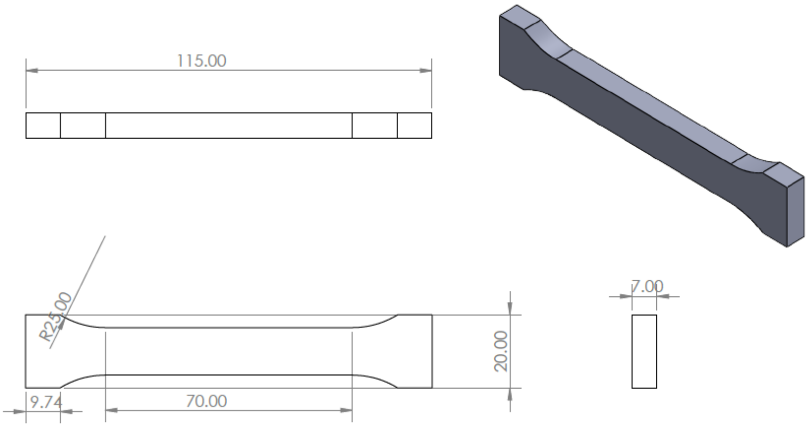


***Figure 2.*** *2D and 3D PETG specimens drawing.*

*Step 2 - Conversion to STL*

The STL (STereoLithography) format is the most common universal file format for 3D models. Developed by 3D Systems in the United States the company that commercialized the first additive manufacturing technology the format was named after their proprietary stereolithography process. Unlike CAD models (as shown in Figure 3), an STL model consists entirely of a triangulated mesh (illustrated in Figure 2) and does not contain any data regarding colour, texture, or material properties.

While a native CAD model retains comprehensive design details and engineering specifications, an STL file encodes solely the raw surface geometry of the object. Because the format relies on a collection of triangles, the quality and smoothness of a 3D print depend heavily on mesh density. For instance, when approximating a perfectly round sphere, a higher number of mesh vertices and triangles yields a smoother surface, whereas a low-density mesh results in a coarse, faceted appearance with visible edges.

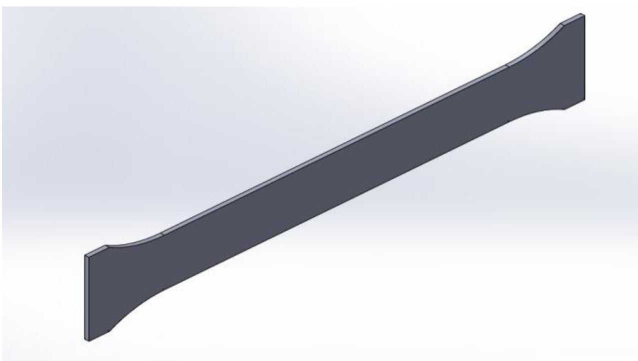

***Figure 3.*** *PETG specimen's 3D solid drawing.*

*Step 3 - Slicing*

The slicing program is an essential software tool that translates a 3D model into machine-readable code for the 3D printer to execute. The software divides the digital model into thin horizontal cross-sections, generating the individual layers required for additive manufacturing. Within the slicing program, users can adjust various parameters to control the quality and mechanical properties of the finished print. Typical parameters include extrusion temperature, infill density, and printing speed.

*Step 4: SLA 3D Printing*

Following the slicing process, the generated file is transferred to the 3D printer. Stereolithography (SLA) 3D printing utilizes a liquid photopolymer resin that is selectively cured by an ultraviolet (UV) laser beam. This curing process is an exothermic polymerization reaction characterized by chemical cross-linking that binds the material into an infusible, insoluble 3D network.

The resin hardens upon exposure to the laser as the build platform incrementally shifts downward (or upward, depending on machine orientation) by a fraction of a millimeter per layer until fabrication is complete. SLA printing delivers exceptional resolution and the ability to produce highly precise components; smaller layer heights yield finer detail and a smoother surface finish. Furthermore, the uncured resin remaining in the vat stays liquid and can be reused, minimizing material wastage. These attributes make SLA printing ideal for applications requiring intricate geometries and high dimensional accuracy.

*Step 5: Post-Processing*

Once printing is finished (as illustrated in Figure 4), the components are not yet ready for final use. SLA printed parts typically retain residual uncured resin on their surfaces. To remove this excess, the parts are rinsed in an alcohol solution. Subsequently, any support structures generated during printing to prevent overhang sagging must be carefully removed by hand to avoid damaging the main geometry.

Finally, the parts are placed in a UV curing chamber for secondary post-curing. Because freshly printed resin models often exhibit a tacky surface finish, additional exposure to UV light and controlled thermal conditions cross-links the remaining polymer chains, strengthening and stabilizing the final component.

***Figure 4.*** *PETG fabricated specimens before testing.*

### 3.2.2. Equipment Overview

The manufacturing and evaluation of the specimens required the 3D printer illustrated in Figure 5 and detailed in Table 2, alongside slicing software to transmit operational commands to the machine. Additionally, a digital microscope was employed to measure discrepancies between the layer height configured in the software and the actual dimensions of the printed output. Detailed descriptions of these components are provided in the subsequent subsections.

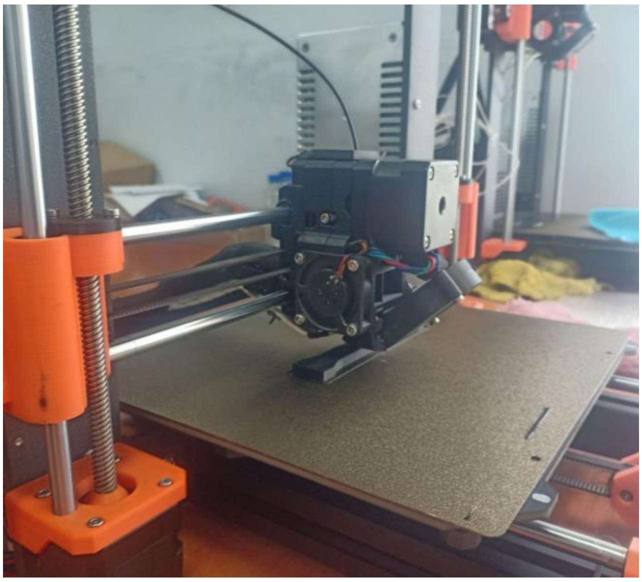

***Figure 5.*** *Prusa i3 MK3S+3D printer machine.*

***Table 2.*** *Specification of Prusa i3 MK3S+3D printer machine.*

| **Printer name** | **Prusa i3 MK3S+3D printer** |
|---|---|
| Mechanism | FDM |
| Filament used | PETG (black) |
| Printing volume | 250x210x200mm |
| Software used for 3D printing | ULTIMATE Cure |
| Nozzle diameter | 0.4mm |

### 3.2.3. Mechanical Characterization of 3D-Printed PETG Samples

To develop a deeper understanding of the material's structural performance, mechanical evaluations were carried out. Given that this material is relatively novel and underexplored in current literature, conducting both tension and compression tests offered a vital advantage. These evaluations enabled the validation and benchmarking of experimental results against existing sparse data, thereby expanding insight into the material profile. Consequently, these trials delivered crucial findings regarding the mechanical behavior of the samples and verified their viability for targeted engineering deployments.

## 3.3. Tensile Test Specimen

Tensile strength defines the peak stress a material can sustain under uniaxial pulling loads, quantifying its resistance to elongation and tension prior to failure. Before securing the sample, the load and plot-axis indicators must be calibrated to zero. The specimen is then carefully aligned and clamped firmly within the grips to ensure complete tab engagement, with one crosshead remaining stationary while the opposite end moves uniaxial until fracture occurs to record the maximum load at break. Tensile evaluations were performed on a hydraulic universal servo testing machine operating at a crosshead speed of 1 mm/min. A total of nine tensile specimens were evaluated using this servo machine, which features a maximum capacity of 65 MPa. This section outlines the complete analytical workflow for the data gathered from tests conducted at the Arba Minch University laboratory (as depicted in Figure 6) across various designated parameters.

***Figure 6.*** *Hydraulic universal servo testing machine.*

The tensile strength is calculated by dividing maximum load (load at break) with an original cross-sectional area (original width × original thickness). Figure 7 shows tensile testing specimens to predict the influence of FDM parameter settings on tensile strength. The following equations are used in the testing analysis.

$$\text{Tensile strength} = \frac{\text{Breaking load(F)}}{\text{Original cross−sectional area}(A_o)} \tag{1}$$


***Figure 7.*** *PETG fractured samples after tensile test.*

*Compression Testing*

As illustrated in Figure 7, a total of nine samples were evaluated utilizing a hydraulic universal servo testing machine (shown in Figure 6) featuring a peak load capacity is 65 MPa. All experimental measurements including applied load, displacement, compressive stress, and final compressive outcomes were logged and exported as a CSV file in Excel. To ensure statistical reliability and account for potential experimental variations, three identical replicates were evaluated for each structural configuration, culminating in the nine total tested specimens. The samples were subjected to quasi-static compression trials under a controlled displacement rate of 0.5 mm/min.

$$\sigma c = Fc/Ac \tag{2}$$

Here σc is the compression stress, Fc is the applied axial load and Ac is the area of cross-section.

***Figure 8.*** *Hydraulic Universal Servo Testing Machine.*


***Figure 9.*** *PETG fractured samples after compression test.*

## 3.4. Experimental Design

### 3.4.1. Design of Experiment Techniques

The Taguchi experimental framework was utilized to evaluate the relative significance of various manufacturing parameters. As a structured optimization technique, it reduces the required trial count through specialized orthogonal arrays while mitigating unpredictable noise disturbances, ensuring that quality parameters are systematically built into processes at the design stage with reduced time and cost burdens [8].

Relying heavily on parametric design, this strategy identifies optimal operating points to maximize performance characteristics while minimizing process variation, using control factors to quickly isolate key variables. To evaluate results, the signal-to-noise (S/N) ratio serves as the primary metric, effectively managing proportional shifts between means and standard deviations [2].

Using Minitab 21, a designed experiment (DoE) layout was constructed utilizing three input variables extrude temperature, infill density, and printing speed each evaluated across three levels. To map this parameter space, a three-factor, three-level orthogonal array configuration ($L_9$) was implemented, mandating nine distinct experimental runs executed at a 95% confidence level. Orthogonal Arrays Pioneered by Sir Ronald Fisher, orthogonal arrays (OAs) minimize the overall testing burden while ensuring that every factor combination appears equally across experimental columns, facilitating efficient multi-parameter evaluation [1].

An $L_9$ array structure dictates nine discrete prototype configurations, where each row corresponds to a specific test condition. Incorporating a minimum of three levels per parameter is crucial for capturing nonlinear or non-monotonic trends, thereby providing higher precision and deeper insight into the relationship between input variables and response outputs. Analysis of Experimental Data Following testing, performance metrics are analyzed using S/N ratios, where the "signal" denotes the target value and the "noise" signifies undesired deviation [11].

Evaluating tensile and compression strengths across the nine-run ($L_9$) orthogonal array layout enabled performance optimization under the "higher-is-better" quality criterion using Minitab 21.0, identifying optimal settings based on standard static optimization S/N formulations. Analysis of Variance (ANOVA) Analysis of variance (ANOVA) was performed at a 95% confidence level (5% significance level) to quantify the percentage contributions of extrude temperature, infill density, and printing speed to the tensile and compression responses [6].

As detailed in Table 3, these operating parameters dictate mechanical performance, and evaluating them via ANOVA and S/N ratios establishes the fundamental relationships governing the mechanical behaviour of the 3D-printed PETG specimens.

$$S/N = -10\log_{10}\left(\frac{1}{n}\sum\frac{1}{y^2}\right) \tag{3}$$

The procedural workflow of grey relational analysis comprises the following phases:

*Step 1:* Establish the experimental data matrix via Design of Experiments (DOE).

*Step 2:* Perform grey relational generation by scaling the raw data to a standardized range between 0 and 1 using normalization formulas, applying equation (4) specifically to optimize (maximize) both tensile and compressive strength metrics [5].

*Higher the better.*

$$x_{1jk} = \left[\frac{y_{ij} - \min(y_{ij})}{\max(y_{ij}) - \min(y_{ij})}\right] \tag{4}$$

Where: $x_{1jk}$ - an experimental run of tensile, and compression strength

$y_{ij}$ –is an experimental run of tensile, and compression strength before preprocessing.

Max $(.y_{ij})$- Maximum value of original data.

Min. $(.y_{ij})$-Minimum value of original data, i=1, 2, 3…m

*Step 3:* Calculation of the grey relational coefficient. To compute the GRC use below equation (5).

$$\gamma\,(x_{0j,}x_{ij}) = \left[\frac{\Delta_{\min} + \zeta\Delta_{\max}}{\Delta_{ij} + \zeta\Delta_{\max}}\right] \tag{5}$$

ζ –Coefficient of distinguishing and its range 0 to 1 but acceptable value was 0.5

*Step 4:* Compute the Grey Relational Grade (GRG) by averaging the grey relational coefficients for every experimental run. The GRG acts as an overall performance indicator for the multi-response optimization process, where the highest grade value identifies the ideal process parameter settings. Through this approach, the multi-objective optimization problem is consolidated into a single GRG metric using equation (6).

$$\gamma_i = \frac{1}{n}\sum_{k=1}^{n}\zeta_i(\mathrm{k}) \tag{6}$$

Where: $\gamma_i$-grey relational grade

n -replication number for response

*Step 5:* Taguchi's method optimizes factor settings for maximum grey relational grade.

### 3.4.2. Selection of Factors

The parameters examined in this study specifically material tensile and compressive strength are influenced by several operational variables, including extrusion temperature, infill density, and printing speed. The selection of these factors for the experimental design was based on previous research reports, literature reviews, material manufacturer recommendations, available machine settings, and relevant technical manuals.

*Selection of Input Parameter Levels*

When determining the specific parameter values presented in Table 3, multiple criteria were evaluated, including literature recommendations, machine technical limitations, material specifications, and prior experimental findings. Because testing every potential variation proved cost-ineffective and time-consuming, a comprehensive review of the literature was conducted to isolate the most influential input factors governing the primary output responses: tensile and compressive strength.

***Table 3.*** *Input parameter of the specimen.*

| Printing parameters | | | Levels | | |
|---|---|---|---|---|---|
| **Input parameters** | **Symbol** | **Unit** | **L -1** | **L -2** | **L -3** |
| Extrude temperature | ET | $0_c$ | 235 | 240 | 245 |
| Infill density | ID | % | 55 | 60 | 65 |
| Printing Speed | $s_p$ | mm/s | 20 | 25 | 30 |

### 3.4.3. Experimental Setup

The experimental analysis began by securely mounting each workpiece on the machine table vice of the hydraulic universal servo testing machine. During the setup, the PETG material, with dimensions of 115x20x7mm, was firmly clamped onto the machine worktable to facilitate the performance experiment. Preceding to the tensile and compression operation, the PETG underwent tension and compression on the hydraulic universal servo testing. Subsequently, the tensile and compression operation was performed using PETG material in different input parameters with their values. These experiments were conducted in the Arba Minch University, utilizing the hydraulic universal servo testing machine. The FDM method was employed to supply the PETG material. The PETG specimens was tensile and compressed using an orthogonal array. Specifically, the Taguchi method $L_9(3^3)$ orthogonal array was selected, along with the corresponding input parameters, for the experiment. A total of 9 experiments were conducted based on the Taguchi method $L_9(3^3)$ orthogonal array, employing different combinations of input parameter levels. In the study, the applied load on the PETG specimen was measured at each step of the experiment. These recorded load values were then utilized to calculate the tensile and compression strength of the specimen. The calculations involved analyzing the specimen's response to the applied load under various values of the process parameters.

By measuring the applied load and calculating the corresponding tensile and compression strength, the research aimed to assess the mechanical properties of the PETG specimen under different experimental conditions. This approach allowed for the evaluation of how variations in the process parameters influenced the specimen's performance and strength characteristics. The recorded load values and subsequent calculations provided valuable data for analyzing the relationship between the process parameters and the mechanical properties of the PETG material. This information could aid in optimizing the process parameters to enhance the overall strength and performance of PETG specimens in various application.

## 4. Result and Discussion

To analyze the behavior of the samples, a mechanical analysis was conducted. Two different types of testing processes were employed to observe the sample's response under loading conditions. The specific details of these testing processes were provided in a subsequent chapter. The laboratory equipment mentioned earlier in the study was utilized to carry out the sample testing and obtain detailed imaging to visualize the sample's structure. These testing processes and imaging techniques allowed for a closer examination of the sample's behavior and characteristics. The optimization results of the PETG specimens confirmed findings reported in the existing literature while also identifying areas that warrant further investigation. The results obtained from the testing provided information such as the peak load at which the samples broke, peak height, and the percentage of compression at each recorded displacement point. All the data obtained from the printed and tested specimens were used to derive specimen parameter data and determine the tensile strength. Based on the results presented in Figure 10 (a) and (b), it can be concluded that the methodology outlined in the previous chapter was successfully implemented. It is important to note that the fracture behavior of the specimens varied due to the different parameters inherent to each specimen, resulting in varying strengths. This analysis and testing phase contributes to the understanding of the sample's mechanical behavior and provides valuable insights into the performance of the PETG specimens. The findings help validate the methodology used and lay the groundwork for further investigation and optimization of the PETG material for various applications.


***Figure 10***. *Result of fracture for PETG specimen after tensile and compression test.*

## 4.1. Design of Experiments

In this investigation, the Taguchi method was applied to optimize sample selection, as detailed in Tables 4 and 5. Due to the evaluation of three distinct process parameters extrude temperature, infill density, and printing speed an $L_9(3^3)$ orthogonal array was implemented, requiring the fabrication of a total of nine test specimens.

***Table 4***. *Design Summary.*

| **Taguchi Array** | **L9 (3^3)** |
|---|---|
| Factors: | 3 |
| Runs: | 9 |

Columns of L9 (3^3) array: 1 2 3

*Orthogonal array*

***Table 1***. *Orthogonal array with assigned factors.*

| **Factors** | **A** | **B** | **C** |
|---|---|---|---|
| | **Column** | | |
| **Trail No** | **1** | **2** | **3** |
| 1 | 1 | 1 | 1 |
| 2 | 1 | 2 | 2 |
| 3 | 1 | 3 | 3 |
| 4 | 2 | 1 | 2 |
| 5 | 2 | 2 | 3 |
| 6 | 2 | 3 | 1 |
| 7 | 3 | 1 | 3 |
| 8 | 3 | 2 | 1 |
| 9 | 3 | 3 | 2 |

***Table 2.*** *Experimental result for tensile (UTS) and compression strength.*

| Run | Input parameters | | | Output parameters | |
|---|---|---|---|---|---|
| | **Extrude temperature** | **Infill density** | **Printing speed** | **Tensile strength (Mpa)** | **Compression strength (Mpa)** |
| 1 | 235 | 55 | 20 | 47.719 | 46.546 |
| 2 | 235 | 60 | 25 | 45.253 | 46.328 |
| 3 | 235 | 65 | 30 | 48.264 | 47.762 |
| 4 | 240 | 55 | 25 | 47.725 | 43.925 |
| 5 | 240 | 60 | 30 | 43.027 | 46.381 |
| 6 | 240 | 65 | 20 | 45.726 | 47.487 |
| 7 | 245 | 55 | 30 | 45.458 | 47.048 |
| 8 | 245 | 60 | 20 | 46.762 | 43.587 |
| 9 | 245 | 65 | 25 | 45.029 | 46.825 |

### 4.1.1. Tensile Strength

*Signal-to-Noise (S/N) Ratio Analysis*

Main Effect Plots for Tensile Strength (MPa)

Figure 11 displays the main effect plots derived from the S/N ratio values across various factor levels for tensile strength. These plots were utilized to determine the optimal setting for each input parameter to maximize tensile performance, adopting the "larger-is-better" quality characteristic. Consequently, the analysis focused on identifying the specific factor levels that yield the highest S/N ratio to establish optimal operating conditions. As evidenced by Figure 11, peak tensile strength was achieved using level 1 (235$^0$C) for extrusion temperature, 55% infill density (level 1), and a 20 mm/s printing speed (level 1). Furthermore, the evaluation indicates that extrusion temperature exerts a more pronounced effect on tensile strength relative to the other parameters when processing PETG. Overall, these findings underscore the critical role of precise parameter selection in optimizing mechanical strength and ensuring target performance outcomes.

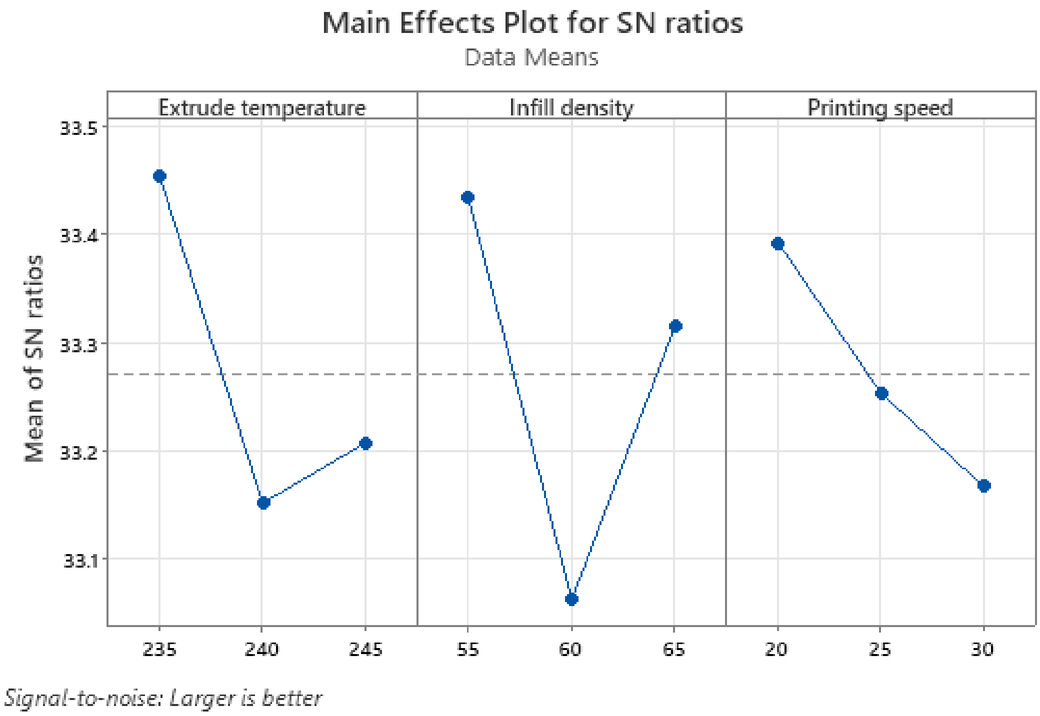


***Figure 11.*** *Main Effect Plot for S/N ratio of tensile strength.*

*Signal-to-Noise Ratio Responses for Tensile Strength*

The primary objective was to maximize tensile strength during testing. Table 7 presents the average response values for each factor level alongside a hierarchy determined by delta statistics, which quantify relative effect sizes by calculating the difference between a factor's maximum and minimum mean values. Minitab 21 automatically assigns ranks based on these delta figures designating Rank 1 to the most dominant factor, followed by Ranks 2 and 3 to reflect the relative influence of each parameter on the outcome.

According to these rankings and delta values, infill density exerts the most significant effect on tensile strength, followed in descending order by extrusion temperature and printing speed. Because higher tensile strength reflects superior mechanical performance under the "larger-is-better" criterion, Figures 12 and Table 7 confirm that peak strength is achieved at the initial settings for each variable: level 1 (235$^0$C) for extrusion temperature, 55% for infill density (level 1), and 20 mm/s for printing speed (level 1). Furthermore, data from Table 7 highlights that infill density plays a pivotal role in securing optimal product quality during tensile testing.

*Larger is better*

***Table 7.*** *Response Table for Means of tensile strength.*

| Level | Extrude temperature | Infill density | Printing speed |
|---|---|---|---|
| 1 | 47.08 | 46.97 | 46.74 |
| 2 | 45.49 | 45.01 | 46.00 |
| 3 | 45.75 | 46.34 | 45.58 |
| Delta | 1.59 | 1.95 | 1.15 |
| Rank | 2 | 1 | 3 |

*Analysis of Variance (ANOVA)*

The ANOVA data presented in Table 8 evaluated the statistical significance of each input variable affecting tensile strength. Serving as an alternative method to assess the impact of process parameters, the ANOVA breakdown (detailed in Table 8) attributes contributions of 19.55% to extrusion temperature, 26.83% to infill density, and 9.18% to printing speed, alongside an error margin of 44.42%. Generated via Minitab 21, the ANOVA results confirm that factors with $P$-values below 0.05 exert a statistically significant effect on tensile strength variance. Consequently, infill density demonstrates the highest relative importance and influence on tensile performance compared to the other parameters, followed by extrusion temperature, whereas printing speed exhibited the minimum effect. These findings align with previous literature, which confirms that mechanical strength is fundamentally governed by process parameters.

***Table 8.*** *Analysis of variance (ANOVA) for tensile strength versus ET, ID and PS.*

| Source | DF | Adj SS | Adj MS | F-Value | P-Value | % of C | Hypothesis |
|---|---|---|---|---|---|---|---|
| Extrude temperature | 2 | 4.348 | 2.174 | 0.44 | 0.045 | 19.548 | Significant |
| Infill density | 2 | 5.967 | 2.983 | 0.60 | 0.028 | 26.827 | Significant |
| Printing speed | 2 | 2.042 | 1.021 | 0.21 | 0.026 | 9.18 | Significant |
| Error | 2 | 9.885 | 4.943 | | | 44.42 | |
| Total | 8 | 22.242 | | | | | |

Regression Analysis: tensile strength ET, ID, and PS

Regression Equation

$$\text{Tensile strength} = 84.7 - 0.133\ \text{Extrude temperature} - 0.063\ \text{Infill density} - 0.182\ \text{Printing speed} \quad (7)$$

### 4.1.2. Compression Strength

Figure 12 illustrates the main effect plots derived from the S/N ratio values across different factor levels for compressive strength. These plots were employed to identify the optimal setting for each input parameter to maximize compression performance under the "larger-is-better" quality criterion. The primary objective was to maximize compressive strength by isolating the factor levels that yield the highest S/N ratio. As demonstrated in Figure 12, optimal compressive strength was achieved using level 1 for extrusion temperature, 65% infill density (level 3), and a 30 mm/s printing speed (level 3). Furthermore, the evaluation indicates that an infill density of 65% exerts a more prominent influence on compressive strength relative to the other parameters for PETG materials. Overall, these findings emphasize the critical role of careful parameter selection in optimizing mechanical behaviour and attaining target performance goals.

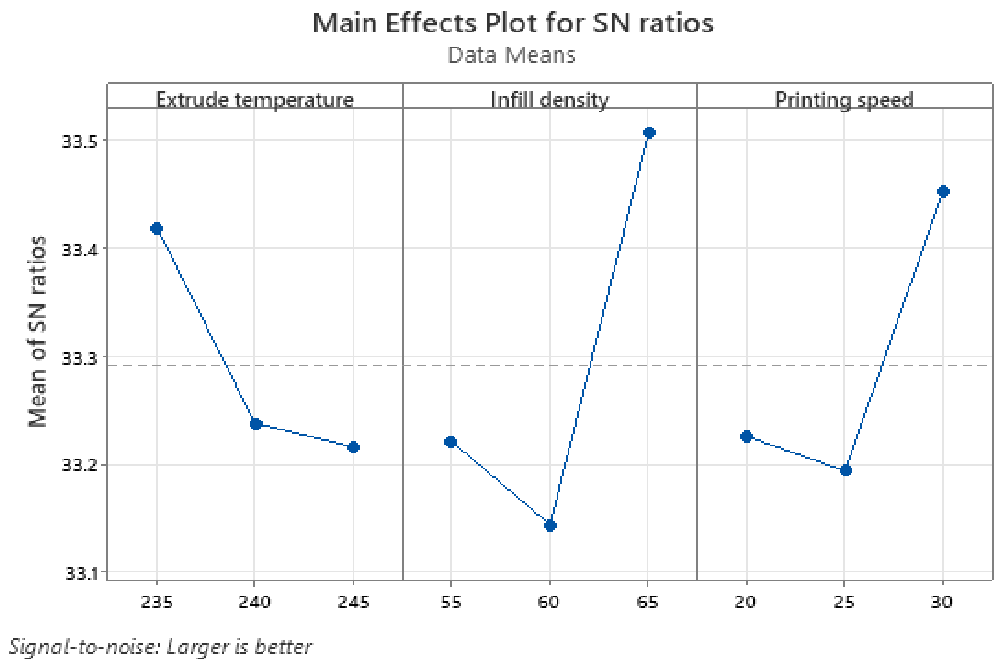


***Figure 12.*** *Main effects plot for S/N ratio of CS.*

*Signal-to-Noise Ratio Responses for Compression Strength*

The primary goal was to maximize compressive strength during testing. Table 6 presents the average response values for each individual factor level, while Table 9 outlines the parameter rankings determined by delta statistics, which measure relative effect magnitudes by finding the difference between a factor's highest and lowest mean values. Utilizing Minitab version 21, parameters are systematically ranked based on these delta figures assigning Rank 1 to the most dominant value, followed sequentially by Ranks 2 and 3 to reflect each variable's relative influence on the response.

According to these rankings and delta values, infill density exerts the most powerful effect on compressive strength, succeeded by printing speed and extrusion technology in descending order. Because higher compressive strength signifies superior quality characteristics under the "larger-is-better" criterion, Figures 12 and Table 9 confirm that peak compressive strength is attained using level 1 for extrusion temperature, level 3 for infill density (65%), and level 3 for printing speed (30 mm/s). Furthermore, data from Table 9 verifies that infill density plays a crucial role in securing optimal product quality during compression evaluations.

***Table 9.*** *Response Table for Means.*

| Level | Extrude temperature | Infill density | Printing speed |
|---|---|---|---|
| 1 | 46.88 | 45.84 | 45.87 |
| 2 | 45.93 | 45.43 | 45.69 |
| 3 | 45.82 | 47.36 | 47.06 |
| Delta | 1.06 | 1.93 | 1.37 |

| Level | Extrude temperature | Infill density | Printing speed |
|---|---|---|---|
| Rank | 3 | 1 | 2 |

*Analysis of Variance (ANOVA)*

The ANOVA data presented in Table 10 was utilized to evaluate the statistical significance of each process parameter on compressive strength, offering an alternative perspective on the influence of printing variables. As detailed in Table 10, the ANOVA breakdown attributes a percentage error of 33.58%, with contributions of 11.69% from extrusion temperature, 35.57% from infill density, and 19.16% from printing speed. Generated via Minitab 21, the ANOVA results confirm that factors with $P$-values below 0.05 exert a statistically significant effect on the variation of compressive strength. Consequently, infill density demonstrates the highest relative importance and impact on compressive performance compared to the other variables, followed sequentially by printing speed, while extrusion temperature exhibited the minimal effect. These conclusions are consistent with previous findings which establish that mechanical strength is fundamentally governed by operating parameters.

***Table 10.** Analysis of Variance (ANOVA).*

| Source | DF | Adj SS | Adj MS | F-Value | P-Value | % of C | Hypothesis |
|---|---|---|---|---|---|---|---|
| Extrude temperature | 2 | 2.031 | 1.016 | 0.35 | 0.022 | 11.687 | Significant |
| Infill density | 2 | 6.181 | 3.091 | 1.06 | 0.048 | 35.57 | Significant |
| Printing speed | 2 | 3.329 | 1.665 | 0.57 | 0.037 | 19.157 | Significant |
| Error | 2 | 5.836 | 2.918 | | | 33.584 | |
| Total | 8 | 17.377 | | | | | |

Regression Analysis: compression strength Value versus extrude temperature, infill density and printing Speed

Regression Equation

$$\text{Compression strength} = 59.5 - 0.106\text{Extrude temperature} + 0.152\text{Infill density} + 0.119\text{Printing speed} \quad (8)$$

## 4.2. Multi Response Optimization

### 4.2.1. Grey Relational Analysis (GRA)

It was performed on the response values mentioned in below Table 11, which aimed to condense the parameters of multiple responses into a single response. Multi response optimization is performed by integrating the Taguchi method and GRA to identify the optimal process parameters.

In GRA, a multi-response problem is converted to an equivalent single-response problem by calculating a Grey grade. Grey relational analysis is used to combine all performance characteristics to be evaluated into a single value that can be used as a single characteristic in optimization problems [9].

***Table 11.** Design of experiment and response of tensile and compression strength.*

| Run | Input parameters | | | Output parameters | |
|---|---|---|---|---|---|
| | Extrude temperature | Infill density | Printing speed | Tensile strength (Mpa) | Compression strength (Mpa) |
| 1 | 235 | 55 | 20 | 47.719 | 46.546 |
| 2 | 235 | 60 | 25 | 45.253 | 46.328 |
| 3 | 235 | 65 | 30 | 48.264 | 47.762 |

| Run | Input parameters | | | Output parameters | |
|---|---|---|---|---|---|
| | Extrude temperature | Infill density | Printing speed | Tensile strength (Mpa) | Compression strength (Mpa) |
| 4 | 240 | 55 | 25 | 47.725 | 43.925 |
| 5 | 240 | 60 | 30 | 43.027 | 46.381 |
| 6 | 240 | 65 | 20 | 45.726 | 47.487 |
| 7 | 245 | 55 | 30 | 45.458 | 47.048 |
| 8 | 245 | 60 | 20 | 46.762 | 43.587 |
| 9 | 245 | 65 | 25 | 45.029 | 46.825 |
| | Min. | | | 43.027 | 43.587 |
| | Max. | | | 48.264 | 47.762 |
| | Max.-Min. | | | 5.237 | 4.175 |

### 4.2.2. Data Preprocessing in Minitab for S/N Ratios

The data analysis commenced after calculating the various response parameters. These parameters were utilized by Minitab software version 21 to calculate the Signal-to-Noise (S/N) ratio for the corresponding responses. During the experimentation process for enhancing process parameters, multiple options were explored to determine the S/N ratio, considering larger-is-better scenarios. Table 11 shows all the performance responses obtained from the Taguchi $L_9$ orthogonal array-based designs.

### 4.2.3. Processing of Data (Normalization)

In this step, the data for the different responses is transformed into a standardized scale ranging from 0 to 1 by using equation (4)

***Table 12.*** *Normalized response for tensile and compression strength.*

| Factors | Output parameters | |
|---|---|---|
| Trial No | Tensile strength (Mpa) | Compressive strength |
| 1 | 0.895 | 0.708 |
| 2 | 0.425 | 0.656 |
| 3 | 1 | 1 |
| 4 | 0.897 | 0.08 |
| 5 | 0 | 0.669 |
| 6 | 0.515 | 0.934 |
| 7 | 0.464 | 0.828 |
| 8 | 0.713 | 0 |
| 9 | 0.382 | 0.775 |
| Max. | 1 | 1 |

### 4.2.4. Defining the Reference Sequence

After normalizing the responses in Table 12, the next step is to calculate the deviations from the reference sequence mentioned in below Table 13.

$$\Delta_{ij}=\|\Delta_{oj}-\Delta_{iijk}\| \quad (9)$$

*Table 13. Absolute value of $\Delta_{ij}$ for tensile and compression strength.*

| Factors | Output parameters | |
|---|---|---|
| Trial No | Tensile strength (Mpa) | Compression strength (Mpa) |
| 1 | 0.105 | 0.292 |
| 2 | 0.575 | 0.344 |
| 3 | 0 | 0 |
| 4 | 0.103 | 0.92 |
| 5 | 1 | 0.331 |
| 6 | 0.485 | 0.066 |
| 7 | 0.536 | 0.172 |
| 8 | 0.287 | 1 |
| 9 | 0.618 | 0.225 |
| $\Delta_{min}$ | 0 | 0 |
| $\Delta_{max}$ | 1 | 1 |

### 4.2.5. Grey Relational Coefficient

Following the initial data pre-processing and normalization, grey relational coefficients (GRC) are computed for every experimental trial by scaling all response values into a 0 to 1 range. The grey grade is subsequently derived by averaging the GRC values across the selected responses. Initially, responses are normalized via equation (4) using the "larger-is-better" criterion, a process known as grey relational generation, where standard test values are compared against normalized data to establish the GRC. Table 12 presents these coefficients, while Table 13 outlines the resulting grey relational grades calculated using equations (5), respectively. The highest grade is designated as Rank 1. Consequently, the Taguchi approach identifies experiment number 9 as yielding the optimal parameter combination for maximizing overall tensile and compression performance across the nine trials. The grey relational grade (GRG) represents the mean GRC for all output responses within a given trial (equation (10)), providing a unified scale to rank all experimental combinations. Through this evaluation, experiment number 3 achieved Rank 1 with a peak GRG of 1, indicating superior overall performance.

*Table 14. Grey relation coefficient (GRC).*

| Factors | Output parameters | |
|---|---|---|
| Trial No | Tensile strength,(Mpa) | Compression strength,(Mpa) |
| 1 | 0.826 | 0.631 |
| 2 | 0.465 | 0.592 |
| 3 | 1 | 1 |
| 4 | 0.829 | 0.352 |
| 5 | 0.333 | 0.601 |

| Factors | Output parameters | |
|---|---|---|
| Trial No | Tensile strength,(Mpa) | Compression strength,(Mpa) |
| 6 | 0.507 | 0.883 |
| 7 | 0.482 | 0.744 |
| 8 | 0.635 | 0.333 |
| 9 | 0.447 | 0.689 |

***Table 15.*** *Total Grey relation coefficient, grade and rank.*

| Trail No | Total of GRC | Grey relational grade | Grey relational rank |
|---|---|---|---|
| 1 | 1.457 | 0.7285 | 2 |
| 2 | 1.057 | 0.5285 | 7 |
| 3 | 2 | 1 | 1 |
| 4 | 1.181 | 0.5905 | 5 |
| 5 | 0.934 | 0.467 | 9 |
| 6 | 1.39 | 0.695 | 3 |
| 7 | 1.226 | 0.613 | 4 |
| 8 | 0.968 | 0.484 | 8 |
| 9 | 1.136 | 0.568 | 6 |

### 4.2.6. Grey Relational Grade (GRG)

The comparability and reference sequences are evaluated to establish the grey relational grades detailed in Table 14. This grading process involves identifying the experimental sequence that most closely mirrors the ideal reference sequence. When analyzing multiple response outputs, a consolidated grey relational grade (GRG) is computed by multiplying each output value by its assigned weight and summing the resulting weighted figures together.

***Table 16.*** *Grey Relational Grade (GRG).*

| Factors | A | B | C | |
|---|---|---|---|---|
| | Column | | | Grey relational grade |
| Trail No | 1 | 2 | 3 | |
| 1 | 1 | 1 | 1 | 0.7285 |
| 2 | 1 | 2 | 2 | 0.5285 |
| 3 | 1 | 3 | 3 | 1 |
| 4 | 2 | 1 | 2 | 0.5905 |
| 5 | 2 | 2 | 3 | 0.467 |
| 6 | 2 | 3 | 1 | 0.695 |
| 7 | 3 | 1 | 3 | 0.613 |

| Factors<br>Trail No | A<br>Column<br>1 | B<br><br>2 | C<br><br>3 | Grey relational grade |
|---|---|---|---|---|
| 8 | 3 | 2 | 1 | 0.484 |
| 9 | 3 | 3 | 2 | 0.568 |
| | Average Grey Relational Grades | | | |
| L - 1 | 0.752 | 0.644 | 0.635 | |
| L - 2 | 0.584 | 0.493 | 0.562 | |
| L - 3 | 0.555 | 0.754 | 0.693 | |
| Min. | 0.555 | 0.493 | 0.562 | |
| Max. | 0.752 | 0.754 | 0.693 | |
| Max.-Min. | 0.197 | 0.261 | 0.131 | |
| Rank | 2 | 1 | 3 | |

### 4.2.7. Analysis of S/N Ratio of Grey Rational Grade (GRG)

The means of the Grey relational grade were calculated for each level of process parameters using data from Table 14 and then it's summarized in the Table 15.

***Table 17.*** *Response table for mean Grey relational grade (GRG).*

| Level | Input parameters<br>Extrude temperature | <br>Infill density | <br>Printing speed |
|---|---|---|---|
| L-1 | 0.752 | 0.644 | 0.635 |
| L-2 | 0.584 | 0.493 | 0.562 |
| L-3 | 0.555 | 0.754 | 0.693 |
| Min. | 0.555 | 0.493 | 0.562 |
| Max. | 0.752 | 0.754 | 0.693 |
| Max.-Min. | 0.197 | 0.261 | 0.131 |
| Rank | 2 | 1 | 3 |

Table 15 indicates that the delta representing the difference between the maximum and minimum Grey Relational Grade (GRG) values is greater for extrusion temperature than for printing speed and infill density. As established by equation (4), a higher GRG signifies superior multi-response quality characteristics. The bolded values in Table 15 highlight the ideal levels for each process parameter, demonstrating that extrusion temperature exerts the most dominant influence on overall performance. Consequently, the optimal parameter combination is identified as follows: extrusion temperature (235$^0$C), infill density (65%), and printing speed (30 mm/s).

### 4.2.8. Regression Analysis

Using Minitab version 21, the collected data was evaluated via multiple regression analysis. Extrusion temperature, infill density, and printing speed served as the independent variables, with tensile and compressive strength acting as the dependent responses. Distinct predictive models were formulated for each mechanical property, yielding specific mathematical equations directly from the regression output.

*Regression Analysis:* tensile strength Vs temperature, infill density and Speed

Optimum parameters obtained from main effect plots of tensile strength are: extrude temperature ($235^0$C), infill density (55%) and printing speed (20mm/s). Hence;

*Regression Equation of tensile strength:*

Tensile strength = 84.7 - 0.133 ET - 0.063 ID-0.182 PS

Tensile strength = 84.7 - 0.133 *235 - 0.063 *55-0.182 *20

Tensile strength = 46.327Mpa

*Regression Analysis of compression strength Vs temperature, infill and Speed*

Optimum parameters obtained from main effect plot of compression strength are: extrude temperature ($235^0$C), infill density (65%) and printing speed (30mm/s). Hence;

*Regression Equation of compression strength:*

Compression strength = 59.5 - 0.106 ET + 0.152 ED+ 0.118 PS (10)

Compression strength = 59.5 - 0.106 *235 + 0.152 *65+ 0.0118*30

Compression strength = 44.826Mpa

### 4.2.9. Validation Testing

As detailed in Table 16, validation tests were performed to verify whether the predicted performance outcomes, derived from the optimized parameter settings, align acceptably with actual experimental findings. The evaluation confirms a strong correlation between the predicted and measured values for both tensile and compressive strength. Verification trials were conducted across two specific scenarios using the optimal parameter configurations:

*Case 1 (Tensile Strength):* Utilizing the ideal settings extrusion temperature at level 1, infill density at level 1, and printing speed at level 1 the measured tensile strength reached 48.264 MPa, showing close alignment with the predicted value of 46.327 MPa generated by equation (7).

*Case 2 (Compressive Strength):* Using the optimized levels of extrusion temperature (level 1), infill density (level 3, 65%), and printing speed (level 3, 30 mm/s), the experimental compressive strength was measured at 47.762 MPa, compared to the predicted value of 44.826 MPa calculated via equation (8).

The complete set of model equations, corresponding experimental results, and associated percentage errors have been computed and are summarized below in Table 16.

$$\text{Percentage error (\%)} = \frac{Experimental\ \ value - Calculated\ \ value}{Experimental\ \ value} \text{x100} \quad (11)$$

*Table 18. Validation test for tensile and compression strength.*

| S. No | Response | Calc. value | Exp. value | P. Error (%) |
|---|---|---|---|---|
| 1 | Tensile strength,(Mpa) | 46.327 | 48.264 | 4.01 |
| 2 | Compression strength,(Mpa) | 44.826 | 47.762 | 6.14 |

The validation test results presented in Table 16, showed that the use of PETG specimens in the tensile and compression produced percentage errors of 4.01Mpa (tensile strength) and 6.14Mpa (compression strength). In general, these percentage errors are considered statistically acceptable due to their values being below 10%. These results validate that a low percentage error was achieved, thereby indicating a strong correlation between the experimental results and the predicted regression models. In addition, the tensile and compression strength operation conducted using the PETG specimens produced better strength compared to the other materials done using the different types of process parameters. These findings revealed that the PETG specimens can serve as a possible substitute for another materials in the tensile and compression operation.

## 5. Conclusion and Recommendation

### 5.1. Conclusion

This study investigated additively manufactured PETG specimens through experimental tensile and compressive testing, utilizing the Taguchi method to evaluate and optimize key process parameters. The work encompassed the design, fabrication, and mechanical assessment of fused deposition modeling (FDM) PETG parts. Key findings and conclusions derived from this work include the tensile performance experimental results and S/N ratio calculations based on the $L_9$ orthogonal array are compiled in Table 6. A peak tensile strength of 48.264 MPa was achieved, confirming that mechanical performance can be significantly enhanced through parameter optimization. Examination of the fractured samples revealed distinct necking and ductile deformation around the crack tips, demonstrating that the PETG tensile specimens possess sufficient elasticity to undergo ductile failure under load. Optimal Tensile Parameters: The ideal process parameter settings for maximizing tensile strength are level 1 for extrusion temperature, 55% for infill density (level 1), and a 20 mm/s printing speed (level 1). Optimal Compressive Parameters configuration for maximizing compressive strength consists of level 1 for extrusion temperature, 65% for infill density (level 3), and a 30 mm/s printing speed (level 3). Tensile ANOVA findings analysis of variance (ANOVA) indicates that all evaluated process parameters significantly influence tensile strength, contributing 19.55% (extrusion temperature), 26.83% (infill density), and 9.18% (printing speed). Notably, infill density (26.83%) emerged as the most dominant factor governing tensile strength enhancement. Compressive ANOVA findings similarly, ANOVA results for compressive performance show significant effects from extrusion temperature (11.69%), infill density (35.57%), and printing speed (19.16%). Infill density (35.57%) was identified as the primary factor driving compressive strength improvements. Validation and Reliability: Confirmation tests utilizing regression models yielded percentage errors of 4.01% for tensile strength and 6.14% for compressive strength, both of which fall well within the statistically acceptable threshold of under 10%. Model Correlation: Validation trials verified a strong correlation between experimental measurements and predicted regression outcomes, though variations in the optimal parameter combinations will alter component performance. The Material Comparison of an experimental findings demonstrate that 3D-printed PETG specimens offer robust mechanical behavior in both tension and compression, highlighting their potential to outperform alternative materials such as ABS and PLA. Grey Relational Optimization: Based on the Taguchi multi-response analysis, experiment number 3 represented the optimal parametric combination (1-3-3), featuring $235^0$C extrusion temperature, 65% infill density, and a 30 mm/s printing speed. Overall, this research successfully accomplished its primary objectives by thoroughly examining the influence of process parameters on the tensile and compressive performance of additively manufactured PETG components.

### 5.2. Recommendations

Further investigation is required to assess and optimize additively manufactured PETG components for broader functional requirements such as hardness, ductility, and stiffness by incorporating alternative materials and varying process parameters. Consequently, future research should broaden the operational ranges of variables like extrusion temperature, infill density, and printing speed, while testing different input values across alternative fabrication techniques to evaluate comparative performance.

## Abbreviations

| | |
|---|---|
| ABS | Acrylonitrile Butadiene Styrene |
| Adj MS | Adjusted Mean Square |
| Adj SS | Adjusted Sum of Square |
| AM | Additive Manufacturing |
| ANOVA | Analysis of Variance |
| CAD | Computer Aided Design |
| DOE | Design of Experiment |
| Eq. | Equation |
| FDM | Fused Deposition Modeling |
| GRA | Grey Relational Analysis |
| GRG | Grey Relational Grade |
| OA | Orthogonal Array |
| PLA | Polylactic Acid |
| S/N | Signal-to-Noise Ratio |
| STL | Stereo Lightography |
| UTM | Universal Testing Machine |

## Acknowledgments

The authors express their gratitude to the publisher and supporting institutions for enabling the sharing and dissemination of this research to the generation.

## Author Contributions

**Abera Ayza Anebo:** Conceptualization, Formal Analysis, Investigation, Methodology, Resources, Software, Validation, Visualization, Writing – original draft

**Temesgen Hailegiorgis Abebe:** Methodology, Resources, Supervision, Visualization

**Devendra Kumar Sinha:** Recourses, Visualization, Writing – review & editing

## Data Availability Statement

Correspondence and material requests should be directed to Abera Ayza Anebo. The publisher maintains a neutral stance regarding jurisdictional claims, territorial boundaries, and political affiliations presented in maps and institutional listings, allowing readers to evaluate the content free from publisher bias.

## Conflicts of Interest

The authors declare no conflicts of interest.

## References

[1] S. Gomez, "Digital Commons @ Georgia Southern An Experimental Study on the Mechanical Properties and Chemical Composition of LCD 3D Printed Specimens," 2023.

[2] M. Simonelli, Y. Tse, and C. J. Tuck, "Microstructure of Ti6Al4V produced by selective laser melting," no. July, 2012, https://doi.org/10.1088/1742-6596/371/1/012084

[3] O. Andersen, M. Vesenjak, T. Fiedler, and U. Jehring, "Experimental and Numerical Evaluation of the Mechanical Behavior of Strongly Ani-so-tropic Light-Weight Metallic Fiber Structures under Static and Dynamic Compressive Loading," 2000, https://doi.org/10.3390/ma9050398

[4] A. Meram and B. Sözen, "Investigation on the manufacturing variants influential on the strength of 3D printed products," vol. x, no. xxxx, pp. 1–21, 2020.

[5] S. Simunovic and O. Ridge, "Energy Absorption in Polymer Composites for Automotive Crashworthiness," no. June, 2017, https://doi.org/10.1177/0021998302036007164

[6] D. O. F. Philosophy and B. Patil, "3D PRINTED SYNTACTIC FOAM," 2019.

[7] A. D. Tura and H. G. Lemu, "Experimental Investigation and Prediction of Mechanical Properties in a Fused Deposition Modeling Process," pp. 1–16, 2022.

[8] D. B. Sitotaw, D. Ahrendt, and Y. Kyosev, "applied sciences Additive Manufacturing and Textiles — State-of-the-Art," pp. 1–21, 2020.

[9] M. Misra, "Additive manufacturing technology of polymeric materials for customized products : recent developments and future prospective," pp. 36398–36438, 2021, https://doi.org/10.1039/d1ra04060j

[10] N. Kladovasilakis, "Study of Mechanical Behavior of Additive Manufactured Lattice Structures to achieve Optimal Product," 2020.

[11] C. Tang, J. Liu, Y. Yang, Y. Liu, S. Jiang, and W. Hao, "Composites Part C : Open Access Effect of process parameters on mechanical properties of 3D printed PLA lattice structures," vol. 3, no. November, 2020, https://doi.org/10.1016/j.jcomc.2020.100076